

Learning Resilient Radio Resource Management Policies with Graph Neural Networks

Navid NaderiAlizadeh, Mark Eisen, and Alejandro Ribeiro

Abstract—We consider the problems of downlink user selection and power control in wireless networks, comprising multiple transmitters and receivers communicating with each other over a shared wireless medium. To achieve a high aggregate rate, while ensuring fairness across all the receivers, we formulate a *resilient* radio resource management (RRM) policy optimization problem with per-user minimum-capacity constraints that *adapt* to the underlying network conditions via learnable slack variables. We reformulate the problem in the Lagrangian dual domain, and show that we can parameterize the user selection and power control policies using a finite set of parameters, which can be trained alongside the slack and dual variables via an unsupervised primal-dual approach thanks to a provably small duality gap. We use a scalable and permutation-equivariant graph neural network (GNN) architecture to parameterize the RRM policies based on a graph topology derived from the instantaneous channel conditions. Through experimental results, we verify that the minimum-capacity constraints adapt to the underlying network configurations and channel conditions. We further demonstrate that, thanks to such adaptation, our proposed method achieves a superior tradeoff between the average rate and the 5th percentile rate—a metric that quantifies the level of fairness in the resource allocation decisions—as compared to baseline algorithms.

Index Terms—Wireless power control, interference channels, resilient radio resource management, Lagrangian duality, primal-dual learning, unsupervised learning, graph neural networks.

I. INTRODUCTION

As 5G network deployments are underway across the world and research studies are already beginning on future 6G technologies, wireless devices and services are becoming more ubiquitous, leading to wireless communication networks that are becoming increasingly complex. These networks will provide connectivity to devices ranging from sensors and cell phones to vehicles, drones, and mixed-reality headsets, shifting the paradigm of how *things* connect together. This will give rise to ultra-dense deployment scenarios, where a massive number of transmissions compete to obtain access to a limited amount of wireless resources.

To deal with these challenges, there has been a plethora of work on the problem of *radio resource management* (RRM), where the goal is to efficiently and optimally allocate the limited time/frequency/spatial resources across the wireless

network. The approaches proposed in the literature use a wide variety of techniques in optimization, information, and game theories in order to attack various RRM sub-problems, including power control, link scheduling, cell association, sub-carrier assignment, and beamforming [3]–[10].

Nevertheless, the aforementioned RRM problems in their most general forms are typically NP-hard, implying that as the network size increases, it becomes more challenging to derive exact optimal solutions to them [11], [12]. That is why most prior work in the literature devise approximate solutions in various regimes of system parameters. With the success of machine learning, and particularly deep learning, over the past few years, learning-based algorithms have emerged to solve challenging problems in wireless communications, including for resource management [13]. As a prominent example, for the class of power allocation problems, several approaches have been proposed that leverage techniques based on supervised, unsupervised, self-supervised, and reinforcement learning, as well as meta-learning and graph representation learning [14]–[29].

A large portion of the prior work on learning-based RRM have considered *unconstrained* optimization of network-wide objective functions, e.g., sum-rate, without any requirements for fair allocation of resources across the network. More recently, the authors in [15], [25] considered *robust* formulations of the RRM problem, where arbitrary constraints can be included in the optimization problem, such as per-user minimum-capacity requirements. However, in wireless networks, channel conditions fluctuate from time to time and from topology to topology. Therefore, even for a constant number of transmitters and receivers within a given network area, a fixed and strict minimum-capacity constraint may not be satisfiable for some of the receivers with poor channel conditions and is hard to define a priori.

In this paper, we intend to take one step further, and learn *resilient* RRM policies that can adapt the system requirements in a controlled way if the network conditions are so extreme that the original constraints render the RRM problem infeasible. In particular, we consider the joint RRM problems of downlink power control and user selection in a wireless network, where the goal is to maximize a network-wide utility function, while ensuring all receivers in the network are treated fairly. We introduce a resilient RRM formulation, where the ergodic long-term average rate of each receiver is forced to be lower-bounded by an *adaptive* minimum-capacity constraint, which is learned via an optimized *slack* variable [30], [31].

We reformulate the aforementioned constrained optimization problem in the Lagrangian dual domain, and propose a

N. NaderiAlizadeh and A. Ribeiro are with the Department of Electrical and Systems Engineering, University of Pennsylvania, Philadelphia, PA 19104, USA (e-mails: {nnaderi, aribeiro}@seas.upenn.edu). M. Eisen is with Intel Labs, Intel Corporation, Hillsboro, OR 97124, USA (e-mail: mark.eisen@intel.com).

This paper was presented in part at the 2020 IEEE International Workshop on Signal Processing Advances in Wireless Communications (SPAWC) [1] and will be presented in part at the 2022 IEEE International Conference on Acoustics, Speech and Signal Processing (ICASSP) [2].

gradient-based primal-dual algorithm to learn optimal RRM policies and their associated optimal constraint slacks, as well as the dual variables corresponding to each constraint in the original optimization problem. We demonstrate how the search over infinite-dimensional RRM policies can be replaced by optimization over a finite set of parameters that can be used to *parameterize* the RRM policies. Under mild assumptions, we prove that such a parameterization only leads to a negligible duality gap, hence enabling us to use the aforementioned primal-dual approach to iteratively update the RRM policy parameters over the course of training. We use a scalable graph neural network (GNN) architecture to parameterize the primal RRM policies, based on a graph topology induced by the underlying instantaneous channel conditions.

We numerically evaluate the performance of our proposed method on a range of system configurations, and show the superior scalability and transferability of the proposed GNN parameterization as compared to baseline methods. We also show how the resilient formulation of the RRM problem trains the per-user slack variables to adapt to the underlying network topology, increasing in value for receivers in poor network conditions, hence relaxing their minimum-capacity constraints.

The rest of this paper is organized as follows. In Section II, we present the system model and formulate the problem. In Section III, we describe the Lagrangian dual formulation and the proposed primal-dual framework. In Section IV, we show how the RRM policies can be parameterized using a shared GNN architecture. In Section V, we present our experimental results. Finally, we conclude the paper in Section VI.

II. SYSTEM MODEL AND PROBLEM FORMULATION

We consider a wireless network with a set of m transmitters $\{\mathbf{T}x_i\}_{i=1}^m$ and a set of n receivers $\{\mathbf{R}x_j\}_{j=1}^n$, where the transmitters intend to communicate with the set of receivers across the network. Before communication begins, a transmitter-receiver association procedure takes place, where each receiver gets associated with a unique transmitter to be served by. We assume that the sets of associated receivers to different transmitters partition the set of receivers throughout the network. In particular, denoting the set of receivers associated with transmitter $\mathbf{T}x_i$ by $\mathcal{R}_i \subseteq \{1, \dots, n\}$, we have

$$\mathcal{R}_i \neq \emptyset, \forall i \in \{1, \dots, m\}, \quad (1a)$$

$$\mathcal{R}_i \cap \mathcal{R}_j = \emptyset, \forall (i, j) \in \{1, \dots, m\}^2 \text{ s.t. } i \neq j, \quad (1b)$$

$$\bigcup_{i=1}^m \mathcal{R}_i = \{1, \dots, n\}, \quad (1c)$$

where (1a) implies that each transmitter has at least one associated receiver, (1b) implies that no receiver is associated with more than one transmitter, and (1c) suggests that the sets of associated receivers to different transmitters cover all the receivers across the network. For a given receiver $\mathbf{R}x_j$, we let $[j]$ denote the index of its unique associated transmitter.

The channel gain between each transmitter $\mathbf{T}x_i$ and each receiver $\mathbf{R}x_j$ in the network is a random variable denoted by h_{ij} . We collect all the channel gains across the network in a matrix, denoted by $\mathbf{H} \in \mathcal{H} \subseteq \mathbb{C}^{m \times n}$. The channel gain matrix \mathbf{H} is assumed to consist of two components: a long-term component

$\mathbf{H}^\ell \in \mathcal{H}^\ell \subseteq \mathbb{R}^{m \times n}$, resulting from signal attenuation from the physical distance between the transmitters and receivers, alongside deviations due to obstacles in the environment, and a short-term fast fading component $\mathbf{H}^s \in \mathcal{H}^s \subseteq \mathbb{C}^{m \times n}$, a result of multi-path propagation and node mobility. Together, these two fading components form the full fading state as the channel matrix $\mathbf{H} = \mathbf{H}^\ell \mathbf{H}^s$. In general, we assume that \mathbf{H}^ℓ is drawn from a joint probability distribution \mathcal{H}^ℓ that governs the random physical deployments of the transmitters and receivers, while \mathbf{H}^s is drawn from a joint probability distribution \mathcal{H}^s that governs the small-scale variations in channel quality. From \mathcal{H}^ℓ and \mathcal{H}^s we further define the distribution of complete channel states \mathcal{H} . We stress that these two random components do not generally vary at the same rate; fast fading \mathbf{H}^s may vary at a millisecond time scale, while large-scale fading \mathbf{H}^ℓ can vary across longer periods of time, e.g., minutes or hours.

Assuming that all transmissions occur at the same time and on the same frequency band, they will cause interference on each other. Therefore, each transmitter needs to set its transmit power so as to optimize a global, network-wide objective, such as sum-throughput. Moreover, assuming that each transmitter can serve a single receiver at each time step, it also needs to decide on which receiver to serve from its set of associated receivers. Given a maximum transmit power of P_{\max} , we denote the vector of power allocation variables by $\mathbf{p} \in [0, P_{\max}]^m$, whose i^{th} component, p_i , represents the transmit power allocated to transmitter $\mathbf{T}x_i$. Furthermore, we let $\gamma \in \{0, 1\}^n$ denote the vector of user selection decisions, whose j^{th} component, γ_j , indicates whether receiver $\mathbf{R}x_j$ has been selected to be served by its associated transmitter $\mathbf{T}x_{[j]}$. Then, the signal-to-interference-plus-noise ratio (SINR) at each receiver $\mathbf{R}x_j$ can be written as

$$\text{SINR}_j(\mathbf{H}, \mathbf{p}, \gamma) = \frac{\gamma_j |h_{[j]j}|^2 p_{[j]}}{N + \sum_{\substack{i=1 \\ i \neq [j]}}^m |h_{ij}|^2 p_i}, \quad (2)$$

where N denotes the noise variance. The Shannon capacity of the link between transmitter $\mathbf{T}x_{[j]}$ and receiver $\mathbf{R}x_j$ is then given by

$$f_j(\mathbf{H}, \mathbf{p}, \gamma) = \log_2(1 + \text{SINR}_j(\mathbf{H}, \mathbf{p}, \gamma)). \quad (3)$$

Due to short-term fading, channel realizations vary over time, implying that the power allocation variables also need to be modified temporally. This motivates considering an ergodic average rate $x_j(\mathbf{H}^\ell)$, which is limited by the ergodic Shannon limit $\mathbb{E}_{\mathbf{H}^s}[f_j(\mathbf{H}, \mathbf{p}, \gamma)]$, to capture the throughput experienced by each receiver $\mathbf{R}x_j$ over a long period of time for a given network configuration specified by large-scale fading \mathbf{H}^ℓ . The goal is to determine power allocation and user selection policies, $\mathbf{p}(\mathbf{H})$ and $\gamma(\mathbf{H})$, that take as input an instantaneous channel realization \mathbf{H} and determine the power levels $\mathbf{p}(\mathbf{H}) = [p_1(\mathbf{H}) \dots p_m(\mathbf{H})]^T$ and user selection decisions $\gamma(\mathbf{H}) = [\gamma_1(\mathbf{H}) \dots \gamma_n(\mathbf{H})]^T$, respectively. We, therefore, formulate the joint power allocation and user selection problem, which we refer to as the *radio resource management* (RRM) problem, as follows, where we seek to

maximize a concave utility $\mathcal{U}(\mathbf{x})$ averaged over large-scale fading configurations, i.e.,

$$\max_{\mathbf{p}, \gamma, \mathbf{x}} \mathbb{E}_{\mathbf{H}^\ell} [\mathcal{U}(\mathbf{x}(\mathbf{H}^\ell))], \quad (4a)$$

$$\text{s.t. } \mathbf{x}(\mathbf{H}^\ell) \leq \mathbb{E}_{\mathbf{H}^\ell} [\mathbf{f}(\mathbf{H}, \mathbf{p}(\mathbf{H}), \gamma(\mathbf{H}))], \quad \mathcal{H}^\ell\text{-a.e.} \quad (4b)$$

$$\mathbf{x}(\mathbf{H}^\ell) \geq f_{\min}, \quad \mathcal{H}^\ell\text{-a.e.} \quad (4c)$$

$$\mathbf{p}(\mathbf{H}) \in [0, P_{\max}]^m, \quad \gamma(\mathbf{H}) \in \Gamma_{n,m}^{\mathcal{R}}. \quad (4d)$$

In (4b)-(4c), \mathcal{H}^ℓ -a.e. implies that the constraints should be satisfied for almost all large-scale fading configurations \mathbf{H}^ℓ drawn from the distribution \mathcal{H}^ℓ . Moreover, in (4d), the user selection constraint set, $\Gamma_{n,m}^{\mathcal{R}}$, is defined as

$$\Gamma_{n,m}^{\mathcal{R}} := \left\{ \gamma(\mathbf{H}) \in \{0, 1\}^n \mid \sum_{j \in \mathcal{R}_i} \gamma_j(\mathbf{H}) = 1, \forall i \in \{1, \dots, m\} \right\}.$$

Observe that in (4c), we specify a constraint on the long-term capacity for each user to be at least f_{\min} for almost any large-scale fading configuration \mathbf{H}^ℓ . These minimum capacity constraints are included so as to avoid allocating all resources to “cell-center” receivers, hence balancing the RRM policies to treat “cell-center” and “cell-edge” receivers *fairly*. We further constrain the user selection policy in (4d) to $\Gamma_{n,m}^{\mathcal{R}}$, where each transmitter is only allowed to serve one of its associated receivers at each time step. Note that the formulation in (4) allows for a transmitter \mathbf{T}_{x_i} to not serve any of its associated receivers at a given time step by setting its transmit power to zero, regardless of the user selection decisions $\{\gamma_j(\mathbf{H})\}_{j \in \mathcal{R}_i}$.

A. Resilient Radio Resource Management

A fundamental challenge exists in tackling the RRM problem in (4) due to the potentially ill-defined minimum capacity constraints used to induce fairness in (4c). Indeed, solving (4) directly requires explicit a priori knowledge of the minimum achievable rate f_{\min} for all network realizations. However, this is generally not known in practice, as complex interference patterns between concurrent transmissions in different network configurations may make some lower bounds infeasible.

We address this problem by introducing a *configuration-dependent slack* term $\mathbf{z}(\mathbf{H}^\ell)$ for the constraints in each configuration, and instead find the optimal RRM policies under the loosened constraint [30], [31]. If for a given user, the generic minimum capacity of f_{\min} is too strict and not achievable due to poor signal and/or strong interference levels, the additional slack $z_i(\mathbf{H}^\ell)$ will address such infeasibility by making the constraint adapt to network conditions. However, any increase in slack z_i will render a solution further from the intended solution of (4), since an arbitrarily large slack will render the fairness constraint irrelevant. We, therefore, impose an additional cost on the slack vector $\mathbf{z}(\mathbf{H}^\ell)$, resulting in the *resilient* formulation of (4), defined as

$$\max_{\mathbf{p}, \gamma, \mathbf{x}, \mathbf{z}} \mathbb{E}_{\mathbf{H}^\ell} \left[\mathcal{U}(\mathbf{x}(\mathbf{H}^\ell)) - \frac{\alpha}{2} \|\mathbf{z}(\mathbf{H}^\ell)\|_2^2 \right], \quad (5a)$$

$$\text{s.t. } \mathbf{x}(\mathbf{H}^\ell) \leq \mathbb{E}_{\mathbf{H}^\ell} [\mathbf{f}(\mathbf{H}, \mathbf{p}(\mathbf{H}), \gamma(\mathbf{H}))], \quad \mathcal{H}^\ell\text{-a.e.} \quad (5b)$$

$$\mathbf{x}(\mathbf{H}^\ell) \geq f_{\min} - \mathbf{z}(\mathbf{H}^\ell), \quad \mathcal{H}^\ell\text{-a.e.} \quad (5c)$$

$$\mathbf{p}(\mathbf{H}) \in [0, P_{\max}]^m, \quad \gamma(\mathbf{H}) \in \Gamma_{n,m}^{\mathcal{R}}, \quad \mathbf{z}(\mathbf{H}^\ell) \geq \mathbf{0}. \quad (5d)$$

We denote the optimal value of (5) by P^* . In (5), along with optimizing the RRM policies \mathbf{p} and γ and ergodic average rates \mathbf{x} , we also optimize the value of the slack \mathbf{z} that optimally trades off the additional utility obtained from relaxing the constraint and the additional cost from the slack itself weighted by $\alpha \geq 0$. The resilient problem is necessarily feasible as $\mathbf{z}(\mathbf{H}^\ell)$ can always be made large to render (5c) satisfied. Indeed, the optimal slack \mathbf{z} *must* be at least as large as the difference between the user-selected goal f_{\min} and the fundamental minimum rate achievable under the given network configuration. By imposing a negative utility on large values of $\mathbf{z}(\mathbf{H}^\ell)$, the optimization of slack variables will implicitly loosen (5c) only enough to maximize a tradeoff between the resulting utility \mathcal{U} and the fairness achieved via a stricter minimum rate constraint.

III. PROPOSED PRIMAL-DUAL LEARNING FRAMEWORK

A. Lagrangian Dual Formulation

To address the existence of constraints in (5), we reformulate the resilient problem in the Lagrangian dual domain. Despite the non-convexity of the capacity function in (3) rendering the resilient program non-convex, it is known that under mild conditions on the channel distributions, the RRM problem exhibits zero duality gap [32]. We can then proceed with the following reformulation without any loss in optimality.

To derive the Lagrangian dual problem, we first introduce the Lagrangian function, with non-negative dual multiplier functions $\boldsymbol{\lambda} : \mathcal{H}^\ell \rightarrow \mathbb{R}_+^n$ and $\boldsymbol{\mu} : \mathcal{H}^\ell \rightarrow \mathbb{R}_+^n$ associated with each constraint in (5), as

$$\begin{aligned} \mathcal{L}(\mathbf{p}, \gamma, \mathbf{x}, \mathbf{z}, \boldsymbol{\lambda}, \boldsymbol{\mu}) &= \mathbb{E}_{\mathbf{H}^\ell} \left[\mathcal{U}(\mathbf{x}(\mathbf{H}^\ell)) - \frac{\alpha}{2} \|\mathbf{z}(\mathbf{H}^\ell)\|_2^2 \right] \\ &\quad - \int_{\mathcal{H}^\ell} \left\{ \boldsymbol{\lambda}(\mathbf{H}^\ell)^T [\mathbf{x}(\mathbf{H}^\ell) - \mathbb{E}_{\mathbf{H}^\ell} [\mathbf{f}(\mathbf{H}, \mathbf{p}(\mathbf{H}), \gamma(\mathbf{H}))]] \right. \\ &\quad \left. + \boldsymbol{\mu}(\mathbf{H}^\ell)^T [f_{\min} - \mathbf{z}(\mathbf{H}^\ell) - \mathbf{x}(\mathbf{H}^\ell)] \right\} g(\mathbf{H}^\ell) d\mathbf{H}^\ell \\ &= \mathbb{E}_{\mathbf{H}^\ell} \left[\mathcal{U}(\mathbf{x}(\mathbf{H}^\ell)) - \frac{\alpha}{2} \|\mathbf{z}(\mathbf{H}^\ell)\|_2^2 \right. \\ &\quad - \boldsymbol{\lambda}(\mathbf{H}^\ell)^T [\mathbf{x}(\mathbf{H}^\ell) - \mathbb{E}_{\mathbf{H}^\ell} [\mathbf{f}(\mathbf{H}, \mathbf{p}(\mathbf{H}), \gamma(\mathbf{H}))]] \\ &\quad \left. - \boldsymbol{\mu}(\mathbf{H}^\ell)^T [f_{\min} - \mathbf{z}(\mathbf{H}^\ell) - \mathbf{x}(\mathbf{H}^\ell)] \right], \quad (6) \end{aligned}$$

where $g(\mathbf{H}^\ell)$ denotes the probability density function of \mathbf{H}^ℓ according to the underlying distribution \mathcal{H}^ℓ . The Lagrangian in (6) provides a single, unconstrained objective function, which we can optimize using gradient-based methods. In particular, we seek to maximize over the so-called primal functions $\mathbf{p}, \gamma, \mathbf{x}, \mathbf{z}$, while subsequently minimizing over the dual functions $\boldsymbol{\lambda}, \boldsymbol{\mu}$, i.e.,

$$D^* := \min_{\boldsymbol{\lambda}, \boldsymbol{\mu}} \max_{\mathbf{p}, \gamma, \mathbf{x}, \mathbf{z}} \mathcal{L}(\mathbf{p}, \gamma, \mathbf{x}, \mathbf{z}, \boldsymbol{\lambda}, \boldsymbol{\mu}). \quad (7)$$

We note that the dual minimization is considered over all non-negative valued functions while the primal maximization is considered over functions of forms given in (5d). Due to the aforementioned zero duality gap property of the RRM

problem, the solution to (7) incurs no loss in optimality relative to the original resilient problem in (5), i.e., $D^* = P^*$.

It is worth elaborating on the resulting functional optimization problem in the dual resilient problem in (7). Observe that solving for the resilient RRM problem in the dual domain requires solving for a total of six functions, or *policies*, which take as input either the large-scale fading state \mathbf{H}^ℓ or the instantaneous fading state $\mathbf{H} = \mathbf{H}^\ell \mathbf{H}^s$. Of most critical importance are the primary resource allocation policies:

- (i) The power allocation policy $\mathbf{p}(\mathbf{H})$ dictating power levels for each transmitter; and,
- (ii) The user selection policy $\gamma(\mathbf{H})$ that determines which receivers are served at each time step.

The remaining four policies take as input a given network configuration \mathbf{H}^ℓ , and define the following:

- (iii) The long-term average rates $\mathbf{x}(\mathbf{H}^\ell)$ obtained from the power allocation and user selection decisions;
- (iv) The slack $\mathbf{z}(\mathbf{H}^\ell)$ that determines the minimum long-term rates achieved in a given network configuration;
- (v) The dual weight policy $\boldsymbol{\lambda}(\mathbf{H}^\ell)$ that corresponds to the constraints on the ergodic long-term average rates; and,
- (vi) The dual weight policy $\boldsymbol{\mu}(\mathbf{H}^\ell)$ that enforces minimum-capacity constraints in the resilient formulation.

Observe that policies (iii)-(vi) serve no purpose during system operation and are only necessary to optimize due to their effect on the optimization of the primal power allocation and user selection policies, $\mathbf{p}(\mathbf{H})$ and $\gamma(\mathbf{H})$.

While the dual formulation in (7) removes the complexity of constraints present in (5), it remains a challenging and often intractable problem to solve in practice. Solving (7) requires a saddle-point functional optimization—i.e., such optimal policies need to be defined for each possible state $\mathbf{H} = \mathbf{H}^\ell \mathbf{H}^s$ and, therefore, (7) can be considered as an infinite-dimensional optimization problem. We address this issue via a *parameterized* dual-based framework for solving the resilient RRM problem in (5), or more specifically, its dual formulation in (7).

B. Parameterization of the Primal RRM Policies

We propose to tackle the statistical regression problem in (7) via *parameterization*, where we replace the infinite-dimensional functional optimization with optimization over a set of parameters of predetermined form. Recall that, in the given problem, we seek to find optimal RRM policies that, once trained, can be generalized to unseen configurations during system operation. We thus replace each of the primal RRM policies $\mathbf{y}(\cdot)$ with a respective parameterization $\mathbf{y}(\cdot; \boldsymbol{\theta}^y)$ that is fully specified by a finite-dimensional parameter vector $\boldsymbol{\theta}^y \in \mathbb{R}^{q_y}$. With this substitution, we obtain the following parameterized Lagrangian function,

$$\mathcal{L}_\theta(\boldsymbol{\theta}^p, \boldsymbol{\theta}^\gamma, \mathbf{x}, \mathbf{z}, \boldsymbol{\lambda}, \boldsymbol{\mu}) := \mathcal{L}(\mathbf{p}(\cdot; \boldsymbol{\theta}^p), \gamma(\cdot; \boldsymbol{\theta}^\gamma), \mathbf{x}, \mathbf{z}, \boldsymbol{\lambda}, \boldsymbol{\mu}). \quad (8)$$

where we have used as inputs to the standard Lagrangian in (6) the parameterized RRM policy definitions. The parameterized dual resilient problem is subsequently defined as

$$D_\theta^* := \min_{\boldsymbol{\lambda}, \boldsymbol{\mu}} \max_{\boldsymbol{\theta}^p, \boldsymbol{\theta}^\gamma, \mathbf{x}, \mathbf{z}} \mathcal{L}_\theta(\boldsymbol{\theta}^p, \boldsymbol{\theta}^\gamma, \mathbf{x}, \mathbf{z}, \boldsymbol{\lambda}, \boldsymbol{\mu}). \quad (9)$$

Unlike the unparameterized dual problem in (7), the *parameterized* dual problem in (9) does not exhibit null duality gap due to the non-convexity of the constraint (5b). Thus, its relation to the original resilient problem in (5) is not immediately evident. However, a connection can be made between these two problems by considering a particular class of parameterizations that are sufficiently dense in their representational abilities. We make the following definition of so-called *near-universal* parameterizations:

Definition 1 A parameterization $\mathbf{y}(\cdot; \boldsymbol{\theta}^y)$ with $\boldsymbol{\theta}^y \in \Theta$ is a *near-universal parameterization* of degree $\epsilon > 0$ for functions in \mathcal{F} if, for any $\mathbf{f} \in \mathcal{F}$, $\exists \boldsymbol{\theta}^y \in \Theta$ such that

$$\mathbb{E}_{\mathbf{H}} \|\mathbf{f}(\mathbf{H}) - \mathbf{y}(\mathbf{H}; \boldsymbol{\theta}^y)\|_\infty \leq \epsilon. \quad (10)$$

Using Definition 1, we may in fact bound the difference between the optimal value obtained via (9) and the optimal value obtained via (5) despite the non-convexities present in the problem when we utilize near-universal parameterizations to represent the primal RRM policies. In proving this result, we need to introduce some restrictions to the problem formulation that we state as assumptions next.

Assumption 1 The probability distribution \mathcal{H} is non-atomic in \mathcal{H} , i.e., for any set $\mathcal{E} \subseteq \mathcal{H}$ of nonzero probability, there exists a nonzero probability strict subset $\mathcal{E}' \subset \mathcal{E}$ of lower probability, $0 < \mathbb{E}_{\mathbf{H}}(\mathbb{I}(\mathcal{E}')) < \mathbb{E}_{\mathbf{H}}(\mathbb{I}(\mathcal{E}))$.

Assumption 2 Slater's condition holds for the resilient problem (5). Especially, there exist variables $\mathbf{x}_0(\mathbf{H}^\ell)$, $\mathbf{p}_0(\mathbf{H})$, and $\gamma_0(\mathbf{H})$ and a strictly positive scalar constant $\sigma > 0$ such that

$$\mathbb{E}_{\mathbf{H}^s} [\mathbf{f}(\mathbf{H}, \mathbf{p}_0(\mathbf{H}), \gamma_0(\mathbf{H}))] - \mathbf{x}_0(\mathbf{H}^\ell) \geq \sigma \mathbf{1}, \forall \mathbf{H}^\ell \in \mathcal{H}^\ell. \quad (11)$$

Assumption 3 The expected performance function $\mathbb{E}[\mathbf{f}(\mathbf{H}, \mathbf{p}(\mathbf{H}), \gamma(\mathbf{H}))]$ is expectation-wise Lipschitz on $\mathbf{p}(\mathbf{H})$ and $\gamma(\mathbf{H})$ for all fading realizations \mathbf{H} . Specifically, for any pair of power allocation policies $\mathbf{p}_1(\mathbf{H}), \mathbf{p}_2(\mathbf{H}) \in [0, P_{\max}]^m$ and user selection policies $\gamma_1(\mathbf{H}), \gamma_2(\mathbf{H}) \in \Gamma_{n,m}^{\mathcal{R}}$, there are constants L_p and L_γ such that

$$\mathbb{E} \|\mathbf{f}(\mathbf{H}, \mathbf{p}_1(\mathbf{H}), \gamma(\mathbf{H})) - \mathbf{f}(\mathbf{H}, \mathbf{p}_2(\mathbf{H}), \gamma(\mathbf{H}))\|_\infty \leq L_p \mathbb{E} \|\mathbf{p}_1(\mathbf{H}) - \mathbf{p}_2(\mathbf{H})\|_\infty, \quad (12)$$

$$\mathbb{E} \|\mathbf{f}(\mathbf{H}, \mathbf{p}(\mathbf{H}), \gamma_1(\mathbf{H})) - \mathbf{f}(\mathbf{H}, \mathbf{p}(\mathbf{H}), \gamma_2(\mathbf{H}))\|_\infty \leq L_\gamma \mathbb{E} \|\gamma_1(\mathbf{H}) - \gamma_2(\mathbf{H})\|_\infty. \quad (13)$$

Assumptions 1–3 place a set of mild assumptions on the scope of (5) and necessary for the subsequent analysis. Assumption 1 states that there are no points of strictly positive probability in the distribution \mathcal{H} , which is a reasonable assumption provided that the channel fading states observed in practice take on a continuum of values. Assumption 2

simply states that service demands can be provisioned with some slack, which is generally realizable in (5) via sufficiently small $\mathbf{x}(\mathbf{H}^\ell)$ and large $\mathbf{z}(\mathbf{H}^\ell)$. Assumption 3 is a continuity statement on each of the dimensions of the expectation of the utility function \mathcal{U} and the rate function \mathbf{f} —we point out this is weaker than general Lipschitz continuity.

As previously mentioned, the duality gap of the original unparameterized problem in (5) is known to be null, implying $D^* = P^*$ [32]. This result does not directly apply to the parameterized dual problem in (9) due to the restriction of the optimization to a finite-dimensional space of learning parameters. However, given validity of Assumptions 1–3 and using a parameterization that is near-universal in the sense of Definition 1, we show that the duality/parameterization gap $|D_\theta^* - P^*|$ between problems (5) and (9) is small, as we formally state next.

Theorem 1 *Consider the resilient RRM problem in (5) and its parameterized Lagrangian dual in (9), in which each of the parameterizations $\mathbf{y}(\cdot; \theta^y)$ is near-universal with degree ϵ_y in the sense of Definition 1 for both primal RRM policies $\mathbf{y} \in \{\mathbf{p}, \gamma\}$. If Assumptions 1–3 hold, then the dual value D_θ^* is bounded by*

$$P^* - \epsilon_p \left(L_f \mathbb{E}_{\mathbf{H}^\ell} \left\| \tilde{\lambda}(\mathbf{H}^\ell) \right\|_1 \right) \leq D_\theta^* \leq P^*, \quad (14)$$

where $\tilde{\lambda}(\mathbf{H}^\ell) = [\lambda^*(\mathbf{H}^\ell); \mu^*(\mathbf{H}^\ell)]$ is the optimal dual policy in (7), $\epsilon_p = \max\{\epsilon_{\mathbf{p}}, \epsilon_\gamma\}$, and $L_f = \max\{L_p, L_\gamma\}$.

Proof: See Appendix A. ■

In Theorem 1, we establish that the solution found via the parameterized dual problem in (9) is close to that of the original unparameterized resilient RRM problem in (5) when near-universal parameterizations are used to represent the primal RRM policies. The degree of this difference is proportional to the degree of near-universality used in the learning parameterization. This allows us to use stochastic primal-dual methods that operate directly on the finite-dimensional, unconstrained problem in (9), as we discuss next.

C. Unsupervised Empirical Primal-Dual Learning

Since we do not have access to the underlying fading distributions \mathcal{H}^ℓ and \mathcal{H}^s , we resort to an *empirical* formulation of the Lagrangian function (8), where the expectations are replaced by empirical sample means. In particular, we generate a set of B large scale fading samples $\{\mathbf{H}_b^\ell\}_{b=1}^B$ according to the distribution \mathcal{H}^ℓ , and we further generate $B \times T$ small-scale fading samples $\{\mathbf{H}_{b,t}^s\}_{b=1, t=1}^{B, T}$ according to the distribution \mathcal{H}^s . This leads to the empirical parameterized Lagrangian

$$\begin{aligned} \hat{\mathcal{L}}_\theta(\theta^p, \theta^\gamma, \mathbf{x}, \mathbf{z}, \lambda, \mu) &= \hat{\mathbb{E}}_{\mathbf{H}^\ell} \left[\mathcal{U}(\mathbf{x}(\mathbf{H}^\ell)) - \frac{\alpha}{2} \|\mathbf{z}(\mathbf{H}^\ell)\|_2^2 \right. \\ &\quad \left. - \lambda(\mathbf{H}^\ell)^T [\mathbf{x}(\mathbf{H}^\ell) \right. \\ &\quad \left. - \hat{\mathbb{E}}_{\mathbf{H}^s} [\mathbf{f}(\mathbf{H}, \mathbf{p}(\mathbf{H}; \theta^p), \gamma(\mathbf{H}; \theta^\gamma))] \right] \\ &\quad \left. - \mu(\mathbf{H}^\ell)^T [f_{\min} - \mathbf{z}(\mathbf{H}^\ell) - \mathbf{x}(\mathbf{H}^\ell)] \right], \end{aligned} \quad (15)$$

where for any functions $\mathcal{F}^\ell : \mathcal{H}^\ell \rightarrow \mathbb{R}$ and $\mathcal{F} : \mathcal{H}^\ell \times \mathcal{H}^s \rightarrow \mathbb{R}$, we define

$$\hat{\mathbb{E}}_{\mathbf{H}^\ell} [\mathcal{F}^\ell(\mathbf{H}^\ell)] := \frac{1}{B} \sum_{b=1}^B \mathcal{F}^\ell(\mathbf{H}_b^\ell), \quad (16)$$

$$\hat{\mathbb{E}}_{\mathbf{H}^s} [\mathcal{F}(\mathbf{H}_b^\ell, \mathbf{H}_{b,t}^s)] := \frac{1}{T} \sum_{t=1}^T \mathcal{F}(\mathbf{H}_b^\ell, \mathbf{H}_{b,t}^s). \quad (17)$$

We can now derive the updates over an iteration index k for each of the primal and dual parameters/variables by either adding or subtracting the partial gradient of $\hat{\mathcal{L}}_\theta(\theta^p, \theta^\gamma, \mathbf{x}, \mathbf{z}, \lambda, \mu)$ with respect to that variable. For power allocation and user selection policies, this gives us the updates,

$$\theta_{k+1}^p = \theta_k^p + \eta_p \delta_k^p, \quad (18)$$

$$\theta_{k+1}^\gamma = \theta_k^\gamma + \eta_\gamma \delta_k^\gamma, \quad (19)$$

where $\eta_p, \eta_\gamma > 0$ denote learning rates corresponding to the primal RRM policy parameters variables θ^p and θ^γ , respectively, and δ_k^p , and δ_k^γ are defined as

$$\begin{aligned} \delta_k^p &= \hat{\mathbb{E}}_{\mathbf{H}^\ell} \left[\nabla_{\theta^p} \left\{ \lambda(\mathbf{H}^\ell)^T \hat{\mathbb{E}}_{\mathbf{H}^s} [\mathbf{f}(\mathbf{H}, \mathbf{p}(\mathbf{H}), \gamma(\mathbf{H}))] \right\} \right], \\ \delta_k^\gamma &= \hat{\mathbb{E}}_{\mathbf{H}^\ell} \left[\nabla_{\theta^\gamma} \left\{ \lambda(\mathbf{H}^\ell)^T \hat{\mathbb{E}}_{\mathbf{H}^s} [\mathbf{f}(\mathbf{H}, \mathbf{p}(\mathbf{H}), \gamma(\mathbf{H}))] \right\} \right]. \end{aligned}$$

As the remaining primal and dual policies are not parameterized, we update the primal and dual variables corresponding to each training configuration separately. In particular, for any $b \in \{1, \dots, B\}$, let $(\mathbf{x}_b, \mathbf{z}_b, \lambda_b, \mu_b)$ respectively denote the ergodic average rate, slack and dual variables corresponding to the b^{th} configuration, i.e.,

$$(\mathbf{x}_b, \mathbf{z}_b, \lambda_b, \mu_b) = (\mathbf{x}(\mathbf{H}_b^\ell), \mathbf{z}(\mathbf{H}_b^\ell), \lambda(\mathbf{H}_b^\ell), \mu(\mathbf{H}_b^\ell)).$$

Then, the ergodic average rate and slack variables corresponding to the b^{th} configuration, $b \in \{1, \dots, B\}$, are updated as

$$\mathbf{x}_{b,k+1} = \mathbf{x}_{b,k} + \eta_{\mathbf{x}} \delta_{b,k}^{\mathbf{x}}, \quad (20)$$

$$\mathbf{z}_{b,k+1} = [\mathbf{z}_{b,k} + \eta_{\mathbf{z}} \delta_{b,k}^{\mathbf{z}}]_+, \quad (21)$$

where $\eta_{\mathbf{x}}, \eta_{\mathbf{z}} > 0$ respectively denote the learning rates corresponding to the ergodic average rate and slack variables \mathbf{x} and \mathbf{z} , $[\cdot]_+ := \max(\cdot, 0)$, and $\delta_{b,k}^{\mathbf{x}}$ and $\delta_{b,k}^{\mathbf{z}}$ are defined as

$$\begin{aligned} \delta_{b,k}^{\mathbf{x}} &= \nabla_{\mathbf{x}_{b,k}} \{ \mathcal{U}(\mathbf{x}_{b,k}) \} + \mu_{b,k} - \lambda_{b,k}, \\ \delta_{b,k}^{\mathbf{z}} &= \mu_{b,k} - \alpha \mathbf{z}_{b,k}. \end{aligned}$$

Finally, we descend on the dual variables using the associated partial gradients of the Lagrangian, i.e., for the b^{th} configuration, $b \in \{1, \dots, B\}$, we have

$$\lambda_{b,k+1} = [\lambda_{b,k} - \eta_\lambda \delta_{b,k}^\lambda]_+, \quad (22)$$

$$\mu_{b,k+1} = [\mu_{b,k} - \eta_\mu \delta_{b,k}^\mu]_+, \quad (23)$$

where $\eta_\lambda, \eta_\mu > 0$ respectively represent learning rates corresponding to the dual variables λ and μ , and $\delta_{b,k}^\lambda$ and $\delta_{b,k}^\mu$ are

Algorithm 1 Primal-Dual Learning of Resilient RRM Policies

- 1: **Input:** Primal and dual learning rates $(\eta_p, \eta_\gamma, \eta_x, \eta_z, \eta_\lambda, \eta_\mu)$, batch size B , # time steps per configuration T .
 - 2: Initialize RRM policy parameters $(\theta_0^p, \theta_0^\gamma)$.
 - 3: Initialize primal and dual variables $(\mathbf{x}_{b,0}, \mathbf{z}_{b,0}, \boldsymbol{\lambda}_{b,0}, \boldsymbol{\mu}_{b,0}) = (\mathbf{0}, \mathbf{0}, \mathbf{0}, \mathbf{0}), \forall b \in \{1, \dots, B\}$.
 - 4: Generate B large-scale fading samples $\{\mathbf{H}_b^\ell\}_{b=1}^B$ according to \mathcal{H}^ℓ .
 - 5: Generate $B \times T$ small-scale fading samples $\{\mathbf{H}_{b,t}^s\}_{b=1, t=1}^{B, T}$ according to \mathcal{H}^s .
 - 6: $k \leftarrow 0$.
 - 7: **while** not converged **do**
 - 8: Update primal RRM policy parameters (see (18)-(19)).
 - 9: Update ergodic long-term average rate and slack variables (see (20)-(21)).
 - 10: Update dual policy parameters (see (22)-(23)).
 - 11: $k \leftarrow k + 1$.
 - 12: **end while**
 - 13: $(\theta^{*p}, \theta^{*\gamma}, \{\mathbf{x}_b^*\}_{b=1}^B, \{\mathbf{z}_b^*\}_{b=1}^B, \{\boldsymbol{\lambda}_b^*\}_{b=1}^B, \{\boldsymbol{\mu}_b^*\}_{b=1}^B) \leftarrow (\theta_k^p, \theta_k^\gamma, \{\mathbf{x}_{b,k}\}_{b=1}^B, \{\mathbf{z}_{b,k}\}_{b=1}^B, \{\boldsymbol{\lambda}_{b,k}\}_{b=1}^B, \{\boldsymbol{\mu}_{b,k}\}_{b=1}^B)$.
 - 14: **Return:** Final primal and dual policy parameters and variables $(\theta^{*p}, \theta^{*\gamma}, \{\mathbf{x}_b^*\}_{b=1}^B, \{\mathbf{z}_b^*\}_{b=1}^B, \{\boldsymbol{\lambda}_b^*\}_{b=1}^B, \{\boldsymbol{\mu}_b^*\}_{b=1}^B)$.
-

defined as

$$\begin{aligned} \delta_{b,k}^\lambda &= \mathbf{x}_{b,k} - \hat{\mathbb{E}}_{\mathbf{H}^s} [\mathbf{f}(\mathbf{H}_b^\ell \mathbf{H}^s, \mathbf{p}(\mathbf{H}_b^\ell \mathbf{H}^s), \gamma(\mathbf{H}_b^\ell \mathbf{H}^s))], \\ \delta_{b,k}^\mu &= f_{\min} - \mathbf{z}_{b,k} - \mathbf{x}_{b,k}. \end{aligned}$$

The primal-dual gradient updates in (18)-(23) successively move the primal and dual variables towards the maximum and minimum points of the Lagrangian dual function, respectively. The complete resilient primal-dual learning algorithm is summarized in Algorithm 1. Observe that the proposed method is *unsupervised* in the sense that we update the primal, slack, and dual variables so as to optimize the objective function and constraints in (5) directly rather than with labeled solutions.

Remark 1 (Structured parameterizations) We note that, in the formulation of the parameterized dual problem in (9) and the subsequent primal-dual algorithm, we make an implicit assumption that the chosen parameterizations properly adhere to the same structure imposed on the unparameterized policies. That is, the primal policy parameterizations take values of associated forms in (5d). Selecting appropriate parameterizations thus requires consideration of these imposed structures, which can typically be enforced by standard output layer functions (e.g., sigmoid, Softmax, ReLU, etc.)—see Section IV-B for details as applied to the RRM problem.

IV. PARAMETERIZING RRM POLICES VIA GRAPH NEURAL NETWORKS

The choice of parameterization functions is critical in achieving optimal RRM policies with good practical performance when solving (5). Fully-connected deep neural networks (DNNs) are a proper choice here, due to their universality property, which states that given enough depth and/or width, they have sufficient expressive power to approximate any function with any desired accuracy [15], [33]. However, despite their theoretical properties, such a parameterization does not scale well—as the parameter dimension (particularly in the input and output layers) grows with number of transmitters and receivers in the network, i.e., m and n —and more critically does not generalize over varying network topologies.

In this section, we discuss and develop a graph neural network (GNN) architecture suitable for solving the RRM problem in networks of any size. In particular, we propose to use GNNs as parameterizations for the primal RRM policies outlined in Section III. Broadly speaking, GNNs can be viewed as a generalization of convolutional neural network (CNN) architectures, whose popularity and practical benefits stem largely from their significantly reduced parameter dimension relative to traditional DNNs, their invariance to input size, and their so-called permutation equivariance. GNNs generalize the convolutional operations performed in CNNs with a convolution performed on arbitrarily structured data [34]–[37]. Moreover, certain GNN architectures are known to satisfy the near-universality assumption in Definition 1 for the class of continuous, equivariant functions [38], thus making them suitable for achieving small error in duality gap.

A. Graph Construction

We consider the data structure in the form of a directed graph $\mathcal{G} = (\mathcal{V}, \mathcal{E}, w)$, where \mathcal{V} denotes the set of graph nodes, connected by directed edges in \mathcal{E} , and $w : \mathcal{E} \rightarrow \mathbb{R}$ is a function that determines the edge weights. More specifically, we define $\mathcal{V} = \{1, \dots, n\}$, where each node represents a receiver. As for the edges, we define \mathcal{E} to include two edge types:

- **Signal edges.** These are self-loops from each node to itself that represent the direct link between each receiver and its serving transmitter. In particular, for each receiver Rx_j , $j \in \{1, \dots, m\}$, with the associated transmitter $\text{Tx}_{[j]}$, there is an edge from node j to itself, i.e., $(j, j) \in \mathcal{E}$, with its weight being a function of the channel gain between transmitter $\text{Tx}_{[j]}$ and receiver Rx_j , i.e., $w(j, j) = e(h_{[j]j})$, where $e : \mathbb{C} \rightarrow \mathbb{R}$ is an arbitrary function.
- **Interference edges.** These are edges representing the interference caused by each transmitter at its un-associated receivers. Specifically, for each two distinct receivers Rx_j and $\text{Rx}_{j'}$ with distinct serving transmitters (i.e., $[j] \neq [j']$), there is an edge from node j to node j' , i.e., $(j, j') \in \mathcal{E}$, with its weight being $w(j, j') = e(h_{[j]j'})$.

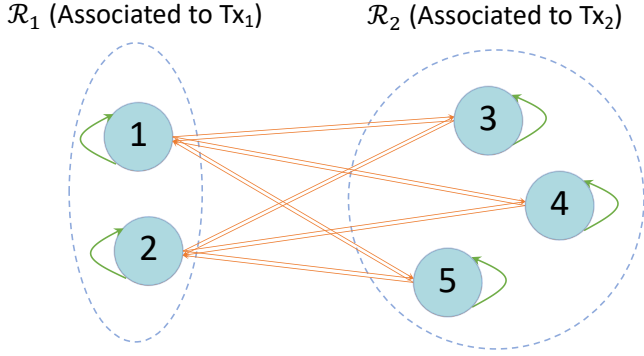


Fig. 1: The weighted directed graph \mathcal{G} in a network with $m = 2$ transmitters and $n = 5$ receivers, where the sets of associated receivers for the two transmitters are given by $\mathcal{R}_1 = \{1, 2\}$ and $\mathcal{R}_2 = \{3, 4, 5\}$. The self-loops (in green) represent the *signal edges*, while the edges between each two pairs of connected receivers (in orange) represent the *interference edges*.

Figure 1 illustrates an example of the graph \mathcal{G} in a network with $m = 2$ transmitters and $n = 5$ receivers, where the sets of receivers served by transmitters Tx_1 and Tx_2 are given by $\mathcal{R}_1 = \{1, 2\}$ and $\mathcal{R}_2 = \{3, 4, 5\}$, respectively. Based on the graph \mathcal{G} , we use a GNN architecture for implementing the primal RRM policies, which we discuss next.

B. GNN Architecture

For each node $v \in \mathcal{V}$, let $\mathbf{y}_v^0 \in \mathbb{R}^{F_0}$ denote the initial *feature vector* corresponding to node v . These feature vectors then go through multiple rounds, i.e., *layers*, of message passing and aggregation along the edges of the graph \mathcal{G} . Denoting the number of such layers by L , for every layer $l \in \{1, \dots, L\}$, we denote the feature vector of each node v by $\mathbf{y}_v^l \in \mathbb{R}^{F_l}$, which is derived as an aggregation of the features of node v and its neighbors from the previous layer, as well as its *incoming* edge weights (including its self-loop), i.e.,

$$\mathbf{y}_v^l = \Psi^l \left(\mathbf{y}_v^{l-1}, w(v, v), \{ \mathbf{y}_u^{l-1}, w(u, v) \}_{u \in \mathcal{N}_v}; \boldsymbol{\theta}^l \right), \quad (24)$$

where $\Psi^l(\cdot; \boldsymbol{\theta}^l)$ denotes a potentially non-linear aggregation function, parameterized through a set of parameters $\boldsymbol{\theta}^l$, and \mathcal{N}_v is defined as the set of neighbors of node v , i.e.,

$$\mathcal{N}_v := \{u \in \mathcal{V} \setminus \{v\} : (u, v) \in \mathcal{E}\}. \quad (25)$$

Each aggregation layer in (24) enables each node to receive information about nodes which are one more hop away of itself. It is clear from the proposed graph construction in Section IV-A that using $L \geq 2$ layers can propagate information from each node to every other node in the graph. After L layers, each node will have a final feature vector $\mathbf{s}_v := \mathbf{y}_v^L \in \mathbb{R}^{F_L}$, which we refer to as its *node embedding*.

We use the aforementioned architecture as the parameterization for the primal power control and user selection policies. In particular, we use a *single* GNN as a *backbone*, i.e., feature extractor, which derives the node embeddings that are subsequently used by *both* the power control and user selection policies in parallel. Such embeddings have been shown to provide semantically-meaningful information when trained and evaluated on wireless power allocation problems [17], [26].

This helps significantly reduce the total number of parameters as opposed to having a separate, independent GNN for each of the two RRM policies. More precisely, after L aggregation layers as in (24), and obtaining the resulting node embeddings for all the nodes in the graph, i.e., $\{\mathbf{s}_v\}_{v \in \mathcal{V}}$, we define the power control and user selection policies as follows:

- **Power control.** For each transmitter Tx_i , $i \in \{1, \dots, m\}$, we derive its transmit power level as

$$p_i(\mathbf{H}) = P_{\max} \cdot \sigma \left(\frac{1}{|\mathcal{R}_i|} \mathbf{b}_p^T \sum_{j \in \mathcal{R}_i} \mathbf{s}_j \right), \quad (26)$$

where $\sigma(\cdot)$ denotes the sigmoid function $\sigma(x) = \frac{1}{1+e^{-x}}$, and $\mathbf{b}_p \in \mathbb{R}^{F_L}$ is a parameter vector mapping the average node embeddings of the receivers associated to Tx_i to a scalar, which is then converted to its allocated transmit power. It is evident from (26) that the resulting allocated power levels satisfy the transmit power constraint $p_i(\mathbf{H}) \in [0, P_{\max}]$.

- **User selection.** For each transmitter Tx_i , $i \in \{1, \dots, m\}$ with the set of associated receivers \mathcal{R}_i , the *estimated* user selection probability for receiver Rx_j , $j \in \mathcal{R}_i$ is derived as

$$\begin{aligned} \gamma_j(\mathbf{H}) &= \text{Softmax}_{\mathcal{R}_i} (\mathbf{b}_\gamma^T \mathbf{s}_j / \tau) \\ &= \frac{\exp(\mathbf{b}_\gamma^T \mathbf{s}_j / \tau)}{\sum_{k \in \mathcal{R}_i} \exp(\mathbf{b}_\gamma^T \mathbf{s}_k / \tau)}, \end{aligned} \quad (27)$$

where $\mathbf{b}_\gamma \in \mathbb{R}^{F_L}$ is a parameter vector and $\tau \in \mathbb{R}_+$ denotes a *temperature* hyperparameter. Using the Softmax operation in (27) ensures that $\sum_{j \in \mathcal{R}_i} \gamma_j(\mathbf{H}) = 1$. However, this will lead to *soft* scheduling decisions, as (27) effectively converts the receiver node embeddings to a scheduling probability distribution over the set of receivers associated with each transmitter. One way to satisfy the *hard* scheduling constraint $\gamma_j(\mathbf{H}) \in \{0, 1\}$ is to use a small-enough temperature $\tau \rightarrow 0$, which in turn “cools” the resulting distribution and reduces its entropy, mimicking an $\arg \max$ operation, i.e.,

$$\gamma_j(\mathbf{H}) \xrightarrow{\tau \rightarrow 0} \mathbb{I} \left(\mathbf{b}_\gamma^T \mathbf{s}_j = \max_{k \in \mathcal{R}_i} \mathbf{b}_\gamma^T \mathbf{s}_k \right), \quad (28)$$

where $\mathbb{I}(\cdot)$ denotes the indicator function. Such low temperature values, however, might lead to unstable gradients when updating the policy parameters as in (19). A more stable alternative is to treat the values of $\{\gamma_j(\mathbf{H})\}_{j \in \mathcal{R}_i}$ as a user scheduling distribution, and sample a user based on this probability distribution, leading to the binary/hard user scheduling decisions $\{\hat{\gamma}_j(\mathbf{H})\}_{j \in \mathcal{R}_i}$. This allows us to replace the user selection policy update in (19) with a *policy gradient* update [15],

$$\boldsymbol{\theta}_{k+1}^\gamma = \boldsymbol{\theta}_k^\gamma + \eta_\gamma \hat{\boldsymbol{\delta}}_k^\gamma, \quad (29)$$

where $\hat{\boldsymbol{\delta}}_k^\gamma$ is a policy gradient estimate, defined as

$$\hat{\boldsymbol{\delta}}_k^\gamma = \hat{\mathbb{E}}_{\mathbf{H}^\ell, \mathbf{H}^s} \left[\left(\boldsymbol{\lambda}(\mathbf{H}^\ell)^T \hat{\mathbf{f}}(\mathbf{H}) \right) \nabla_{\boldsymbol{\theta}^\gamma} \log \pi_{\gamma, \hat{\gamma}}(\mathbf{H}) \right]. \quad (30)$$

In (30), $\hat{\mathbf{f}}(\mathbf{H}) = \mathbf{f}(\mathbf{H}, \mathbf{p}(\mathbf{H}), \hat{\gamma}(\mathbf{H}))$ represents the observed

performance function, and $\pi_{\gamma, \hat{\gamma}}(\mathbf{H})$ is defined as

$$\pi_{\gamma, \hat{\gamma}}(\mathbf{H}) := \prod_{i=1}^m \prod_{j \in \mathcal{R}_i} \gamma_j(\mathbf{H})^{\hat{\gamma}_j(\mathbf{H})}, \quad (31)$$

which represents the joint probability of the selected receivers by all the transmitters across the network. Such updates form the basis for the REINFORCE method in the reinforcement learning literature [39]–[41].

C. Permutation Equivariance of GNN-Based Policies

A key feature of GNNs that make them well suited for learning in wireless networks lies in a structural property called *permutation equivariance*. Permutation equivariance implies that any relabeling of the indices of the nodes in the graph \mathcal{G} will result in an equally-permuted set of output node embeddings. More formally, let $\Pi \in \{0, 1\}^{n \times n}$ denote a *permutation matrix*, which satisfies

$$\Pi \mathbf{1}_n = \Pi^T \mathbf{1}_n = \mathbf{1}_n, \quad (32)$$

where $\mathbf{1}_n$ denotes a vector of size n with all entries equal to one. Moreover, let $\mathbf{A} \in \mathbb{R}^{n \times n}$ denote the weighted adjacency matrix of the graph \mathcal{G} ; i.e., for any $(u, v) \in \mathcal{V}^2$,

$$A_{ij} = \begin{cases} w(u, v) & \text{if } (u, v) \in \mathcal{E}, \\ 0 & \text{o.w.} \end{cases} \quad (33)$$

In addition, let $\mathbf{Y} := [\mathbf{y}_1^{0T} \dots \mathbf{y}_n^{0T}]^T \in \mathbb{R}^{n \times F_0}$ and $\mathbf{S} := [\mathbf{s}_1^T \dots \mathbf{s}_n^T]^T \in \mathbb{R}^{n \times F_L}$ denote the arrays of initial node features and final node embeddings, respectively. Then, we can state the following proposition.

Proposition 1 Consider a GNN operator Ψ , which maps the initial node features \mathbf{Y} over a weighted adjacency matrix \mathbf{A} to a set of node embeddings \mathbf{S} through L aggregation layers as in (24), denoted by $\mathbf{S} = \Psi(\mathbf{Y}, \mathbf{A})$. Then, for any given permutation matrix Π , we have

$$\Psi(\Pi \mathbf{Y}, \Pi \mathbf{A} \Pi^T) = \Pi \Psi(\mathbf{Y}, \mathbf{A}). \quad (34)$$

Proof: See Appendix B ■

Note that the permutation equivariance property highlighted in Proposition 1 directly translates to the permutation equivariance of both the GNN-based power control and user selection policies defined in Section IV-B, since the mappings from the node embeddings to the policy outputs, as mentioned in (26)–(27), are local operations that are insensitive to permutations. This property is especially valuable for resource management in wireless networks as it can facilitate the training of a GNN to operate over many different geometric configurations of the transmitters and receivers in the network, which will invariably change over time in practice. In the next section, we will demonstrate the effectiveness of using GNNs to achieve strong performance over a wide range of network configurations.

V. EXPERIMENTAL EVALUATION

A. Wireless Network Settings

We consider wireless networks with $m \in \{4, 6, 8, 10\}$ transmitters and $n \in \{40, 60, 80, 100\}$ receivers, dropped randomly within a $500\text{m} \times 500\text{m}$ square area. We drop the transmitters and receivers uniformly at random within the network area, and ensure minimum pairwise distances of 35m and 10m for each transmitter-transmitter and transmitter-receiver pair, respectively. The long-term channel model, \mathbf{H}^ℓ , consists of a log-normal shadowing component with 7 dB standard deviation, as well as a standard dual-slope path-loss model [42], [43], which defines the path-loss at distance d as

$$\text{PL}(d) = \begin{cases} K_0 d^{\alpha_1} & \text{if } d \leq d_{bp}, \\ K_0 \frac{d^{\alpha_2}}{d_{bp}^{\alpha_2 - \alpha_1}} & \text{o.w.} \end{cases} \quad (35)$$

In (35), we set $K_0 = 39$ dB, $d_{bp} = 100\text{m}$, $\alpha_1 = 2$, and $\alpha_2 = 4$. We also model the short-term Rayleigh fading, \mathbf{H}^s , using the sum of sinusoids (SoS) technique [44] with a pedestrian speed of 1m/s. The bandwidth is taken to be 10 MHz, the noise power spectral density is assumed to be -174 dBm/Hz, and the maximum transmit power is taken to be $P_{\max} = 10$ dBm.

We adopt a max-SINR user association strategy [45], where the set of receivers associated to each transmitter \mathbf{T}_{x_i} , $i \in \{1, \dots, m\}$, is defined as

$$\mathcal{R}_i = \left\{ j \in \{1, \dots, n\} : i = \arg \max_{i' \in \{1, \dots, m\}} |h_{i'j}^\ell|^2 \right\}, \quad (36)$$

where $h_{i'j}^\ell$ denotes the long-term channel gain between between transmitter $\mathbf{T}_{x_{i'}}$ and receiver \mathbf{R}_{x_j} . Once user association is complete, each configuration is run for 200 time steps, where the first 100 time steps are used as a warm-up period to stabilize the receiver rates, in which all transmitters use full transmit power P_{\max} and serve their associated receivers in a round-robin fashion, and the second $T = 100$ time steps are used to train and evaluate the models.

B. Learning Parameters

In order to implement the primal RRM policies using a GNN parameterization, we use the local extremum operator proposed in [46], where the aggregation layer (24) is given by

$$\mathbf{y}_v^l = \mu \left(\mathbf{y}_v^{l-1} \boldsymbol{\theta}_1^l + \sum_{u: (u,v) \in \mathcal{E}} w(u, v) \left(\mathbf{y}_v^{l-1} \boldsymbol{\theta}_2^l - \mathbf{y}_u^{l-1} \boldsymbol{\theta}_3^l \right) \right).$$

Here, $(\boldsymbol{\theta}_1^l, \boldsymbol{\theta}_2^l, \boldsymbol{\theta}_3^l)$ are learnable parameters, all in $\mathbb{R}^{F_{l-1} \times F_l}$, and $\mu(\cdot)$ represents a LeakyReLU non-linearity (with a negative slope of 10^{-2}). We use $L = 2$ hidden layers, each with 64 features, i.e., $F_1 = F_2 = 64$, and we set the temperature hyperparameter for the user selection policy to $\tau = 10$.

We use the normalized channel gains in dB to determine the edge weights. In particular, for a given channel matrix \mathbf{H} and for a signal/interference element h_{ij} in \mathbf{H} , we define the edge weight function $e(\cdot)$ as

$$e(h_{ij}) = \frac{\log \left(\frac{P_{\max}}{N} |h_{ij}|^2 \right)}{\left(\sum_{i'=1}^m \sum_{j'=1}^n \left[\log \left(\frac{P_{\max}}{N} |h_{i'j'}|^2 \right) \right]^2 \right)^{1/2}}. \quad (37)$$

As for the initial node features, we use a scalar feature for each node, i.e., $F_0 = 1$, and set it to the *proportional-fairness* (PF) ratio of the corresponding receiver. In particular, at each time step t , for each receiver Rx_j , $j \in \{1, \dots, n\}$, we define the initial node feature vector of node j at that time step as $\mathbf{y}_j^0(t) = [\text{PF}_j(t)]$, where

$$\text{PF}_j(t) := \frac{\hat{f}_j(t)}{\bar{f}_j(t)}. \quad (38)$$

In (38), $\hat{f}_j(t)$ denotes the *estimated* rate of receiver Rx_j at time step t , defined as

$$\hat{f}_j(t) = \log_2 \left(1 + \frac{|h_{[j]j}|^2 P_{\max}}{N + P_{\max} \sum_{\substack{i=1 \\ i \neq [j]}}^m |h_{ij}|^2} \right), \quad (39)$$

and $\bar{f}_j(t)$ denotes the *exponential moving-average rate* of receiver Rx_j at time step t , which is recursively updated as

$$\bar{f}_j(t) = (1 - \beta)\bar{f}_j(t-1) + \beta f_j(t), \quad (40)$$

with $f_j(t)$ denoting the actual achieved rate of the receiver at time step t , and $\beta \in [0, 1]$ denoting the inverse averaging window length. In our experiments, we set $\beta = 0.05$. Resource management based on the PF ratios have been proven to lead to fair resource allocation decisions across the network [47].

We utilize a sum-rate network utility function $\mathcal{U}(\mathbf{x}(\mathbf{H}^\ell)) = \sum_{i=1}^n x_i(\mathbf{H}^\ell)$, we set the minimum capacity to $f_{\min} = 1$ bps/Hz, and we use a value of $\alpha = 10^{-2}$ as the slack norm regularization parameter.

During training, we use 256 training configurations and 128 validation configurations. We train the primal and dual parameters/variables over a total of 400 epochs using a batch size of 64. After each training epoch, we evaluate the trained RRM policies on the 128 validation configurations and save the policies that lead to the highest 5th percentile rate. During the evaluation phase, we test the saved policies on a separate set of 128 test configurations. We initialize the primal RRM policy learning rates as $\eta_{\mathbf{p}} = \eta_{\gamma} = 10^{-3}$ and the rest of the learning rates as $\eta_{\mathbf{x}} = \eta_{\mathbf{z}} = \eta_{\lambda} = \eta_{\mu} = 1$. Every 50 epochs, we decrease all of the learning rates by $\frac{1}{2}$. We implement the entire training and evaluation procedures using the PyTorch Geometric library [48].¹

C. Baseline Methods

We compare the performance of our proposed method with two baselines, namely full reuse and ITLinQ [7], [49]. In the full reuse method, all transmitters transmit with full power at each time step, whereas in ITLinQ, a subset of transmitters are scheduled at each time to transmit with full power based on the information-theoretic optimality condition for treating interference as noise [50]. In both baselines, we use a PF-based

user selection policy, where at time step t , for each transmitter Tx_i , $i \in \{1, \dots, m\}$, the user selection decisions are set to

$$\gamma_j(t) = \mathbb{I} \left(j = \arg \max_{k \in \mathcal{R}_i} \text{PF}_k(t) \right), \quad \forall j \in \mathcal{R}_i, \quad (41)$$

where we have replaced the dependency of γ_j on the instantaneous channel matrix \mathbf{H} with the time step index t for clarity.

D. Performance on Identical Training and Evaluation Settings

Figure 2 compares the performance of the proposed method and the baseline methods in terms of mean and 5th percentile rates for networks with $m \in \{4, 6, 8, 10\}$ transmitters and $n = 40$ receivers. For each value of m , the evaluation results are based on the model trained with the same number of transmitters. As the results show, while slightly underperforming ITLinQ in terms of mean rate, the proposed method significantly outperforms both baselines in terms of the 5th percentile rate. This demonstrates how the resilient formulation of the RRM problem leads to a considerably fairer resource allocation across all the receivers, balancing the rates achieved by “cell-center” and “cell-edge” receivers.

To cast more light on the role of the slack variable in the primal-dual learning process, Figure 3 illustrates the evolution of the average slack variable during the training procedure for different values of m . As the number of transmitters, i.e., m , increases, each of the $n = 40$ receivers has a higher probability of being served by a closer transmitter, hence the network will be less interference-limited. This is precisely reflected in Figure 3, where the average slack variable converges to a smaller value for networks with a larger number of transmitters, hence leading to more strict minimum-capacity requirements.

E. Transferability to Larger Network Sizes

While the results in Section V-D demonstrated the performance of the proposed method for similar training and evaluation network sizes, as we mentioned in Section IV, one of the main benefits of GNNs is their *size invariance*. In other words, a GNN trained on a given network size can be evaluated on any arbitrary network size. Thus, here we evaluate the *transferability* of the trained RRM policies, i.e., how policies trained on smaller networks perform in larger configurations.

In Figure 4, we consider the RRM policies trained on networks with $m = 4$ transmitters and $n = 40$ receivers. Once training is complete, we then freeze those policies and evaluate them on networks with $n \in \{40, 60, 80, 100\}$ receivers and $m = n/10$ transmitters. As the figure shows, the proposed method transfers significantly well to graphs of more than twice the size, maintaining its 5th percentile rate gains over the baseline methods. This demonstrates the inherent capability of GNN parameterizations that make the resulting models insensitive to the underlying network size, as opposed to regular DNN-based parameterizations, which become unusable if the network size during execution is different from the ones on which the policies have been trained.

¹Our code is available at https://github.com/navid-naderi/Resilient_RRM_GNN.

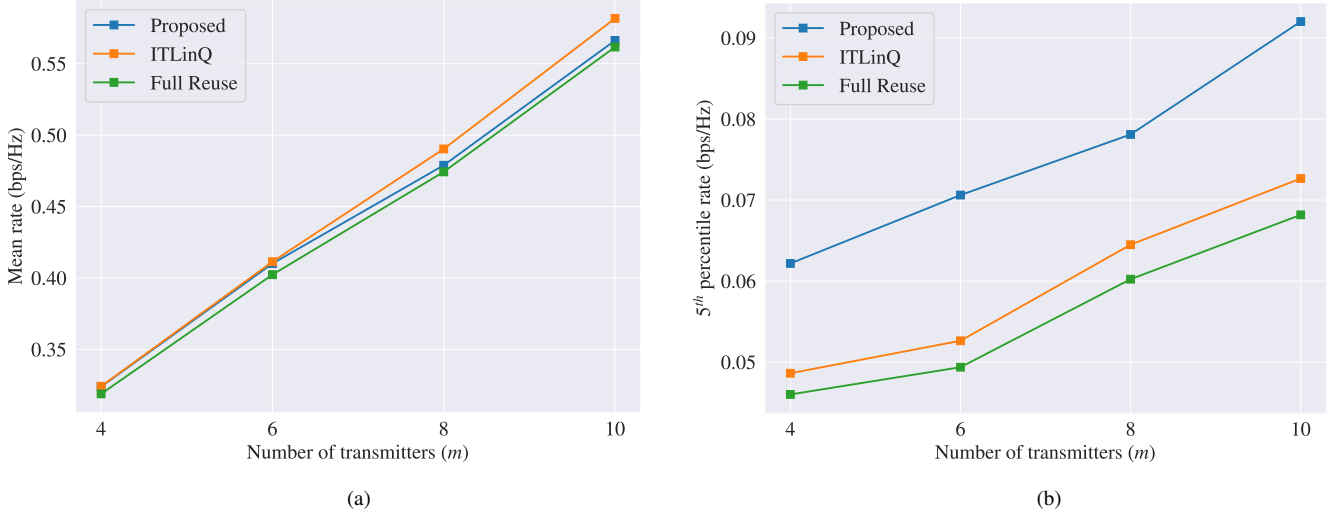


Fig. 2: Comparison of the proposed method with baseline algorithms in terms of (a) mean rate and (b) 5th percentile rate for networks with $m \in \{4, 6, 8, 10\}$ transmitters and $n = 40$ receivers, where for each scenario, the value of m was kept fixed during both training and evaluation.

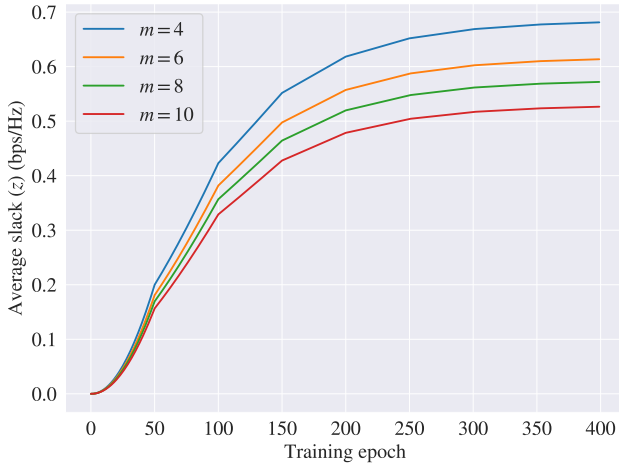


Fig. 3: Evolution of the average slack variable during training for networks with $m \in \{4, 6, 8, 10\}$ transmitters and $n = 40$ receivers.

F. Interpretation of Slack Values as a Function of Underlying Network Conditions

Our main motivation for the resilient formulation of the RRM problem was to learn RRM policies that adaptively relax the minimum-capacity constraints for receivers that are not in desirable channel conditions. To verify that the trained policies have indeed learned such relaxations properly, we can visualize the learned slack variables as a function of network conditions for each receiver in the training set.

To that end, we consider the primal-dual training procedure in networks with $m = 4$ transmitters, and $n = 40$ receivers. For each receiver $Rx_j, j \in \{1, \dots, n\}$, in each configuration, we retrieve its final slack level $z_j(\mathbf{H}^\ell)$, alongside three other quantities that reflect its channel conditions, namely:

- its large-scale signal-to-noise (SNR), $P_{\max} |h_{[j]j}^\ell|^2 / N$;
- its dominant large-scale interference-to-noise ratio (INR), $\max_{i \neq [j]} P_{\max} |h_{ij}^\ell|^2 / N$; and,

- its dominant large-scale signal-to-interference ratio (SIR), $|h_{[j]j}^\ell|^2 / \max_{i \neq [j]} |h_{ij}^\ell|^2$.

Figure 5a shows a scatter plot of the slack values as a function of the large-scale SIR in dB, normalized as in (37). As the figure shows, the slack values have a general downward trend with increased SIR, which is as expected: Receivers with higher large-scale SIR levels have more favorable channel conditions and, therefore, need less relaxation for their corresponding minimum-capacity constraints. Moreover, Figure 5b illustrates an interpolated heatmap of the slack value as a function of the normalized SNR and dominant INR levels. The learned slack values are generally largest around the origin (low SNR levels) or the identity line (low SIR levels), which shows how the resilient formulation of the RRM problem provides a granular control over the minimum-capacity requirements for different users across the network.

VI. CONCLUDING REMARKS

We considered the problem of downlink power control and user selection in wireless networks with multiple interfering transmitters, which intend to serve multiple receivers. To balance fairness across receivers while maximizing their average achieved rate, we formulated a constrained optimization problem with per-user minimum-capacity requirements. We showed how the aforementioned radio resource management (RRM) policies can be made *resilient* through the introduction of slack variables, which relax the minimum-capacity constraints for receivers in poor network conditions. We reformulated the problem in the Lagrangian dual domain and introduced parameterizations for the RRM policies to resolve the challenge of infinite-dimensional functional optimization. We specifically used a graph neural network (GNN) parameterization for the RRM policies, and we proposed a primal-dual approach to train the GNN parameters, as well as the remaining primal and dual variables, via iterative stochastic gradient

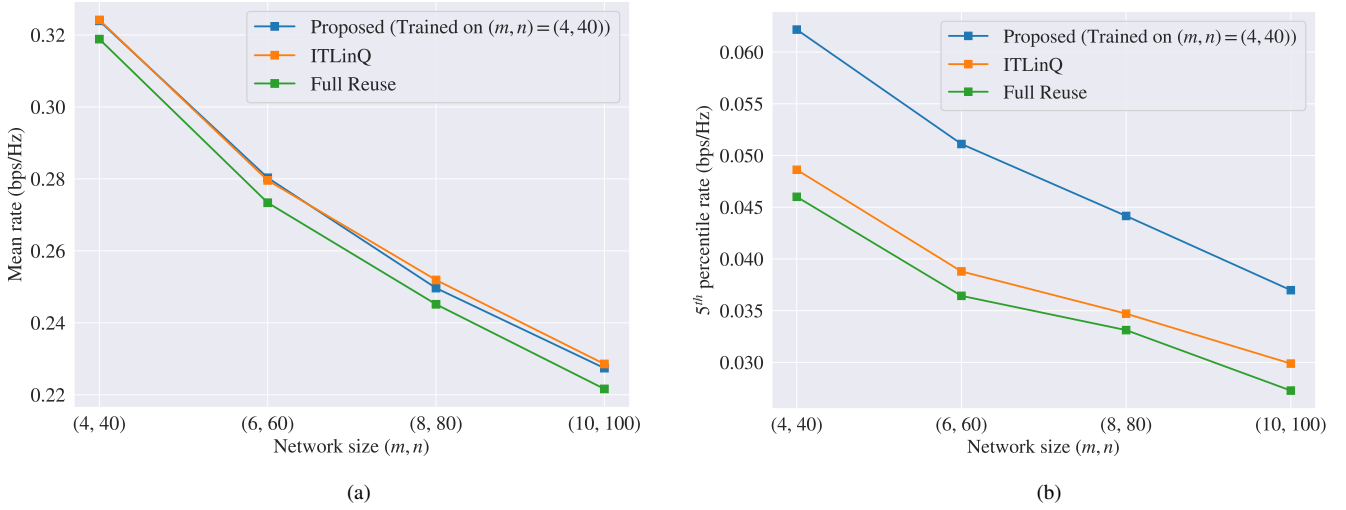


Fig. 4: Transferability of the proposed method, where the model trained on networks with $m = 4$ transmitters and $n = 40$ receivers is evaluated on larger network configurations. The transferability performance of the proposed method is compared with baseline algorithms in terms of (a) mean rate and (b) 5th percentile rate.

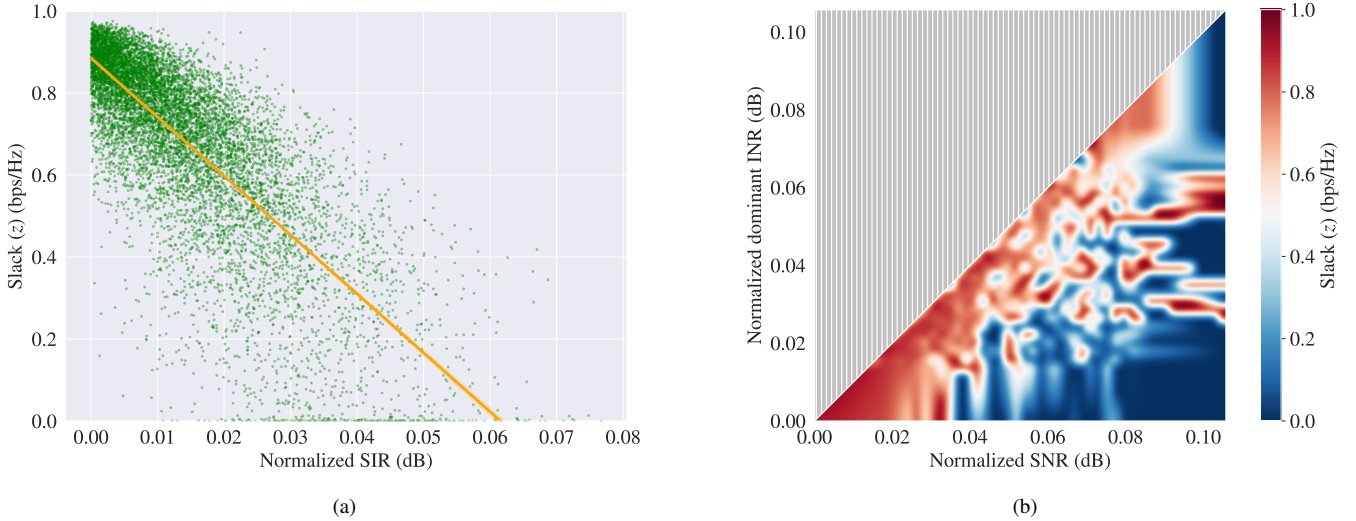


Fig. 5: (a) Scatter plot of the per-receiver slack values versus the normalized signal-to-interference ratio (SIR) levels, and (b) heatmap of (interpolated) per-receiver slack values as a function of the normalized signal-to-noise ratio (SNR) and the dominant interference-to-noise ratio (INR). Both plots are based on final slack values for the proposed model trained on networks with $m = 4$ transmitters and $n = 40$ receivers. The SIR in (a) and the dominant INR in (b) reflect only the strongest interferer at each receiver. The SNR, INR, and SIR values are calculated based on the long-term fading states in \mathbf{H}^ℓ .

updates. Experimental results demonstrated the superiority of our proposed algorithm compared to baseline methods in terms of the trade-off between average and 5th percentile user rates, even in scenarios where the network size during evaluation was more than twice as large as the ones seen during training. We further showed how the resulting slack variables adapt themselves to the underlying network configuration, increasing in value—thereby relaxing the minimum-capacity constraints—for receivers with unfavorable channel conditions.

REFERENCES

- [1] N. Naderializadeh, M. Eisen, and A. Ribeiro, “Wireless power control via counterfactual optimization of graph neural networks,” in *2020 IEEE 21st International Workshop on Signal Processing Advances in Wireless Communications (SPAWC)*. IEEE, 2020, pp. 1–5.
- [2] —, “Adaptive wireless power allocation with graph neural networks,” to appear at *2022 IEEE International Conference on Acoustics, Speech and Signal Processing (ICASSP)*. IEEE, 2022.
- [3] R. Madan, J. Borran, A. Sampath, N. Bhushan, A. Khandekar, and T. Ji, “Cell association and interference coordination in heterogeneous LTE-A cellular networks,” *IEEE Journal on Selected Areas in Communications*, vol. 28, no. 9, pp. 1479–1489, 2010.
- [4] Q. Shi, M. Razaviyayn, Z.-Q. Luo, and C. He, “An iteratively weighted MMSE approach to distributed sum-utility maximization for a MIMO interfering broadcast channel,” *IEEE Transactions on Signal Processing*, vol. 59, no. 9, pp. 4331–4340, 2011.
- [5] W. Yu, T. Kwon, and C. Shin, “Multicell coordination via joint scheduling, beamforming, and power spectrum adaptation,” *IEEE Transactions on Wireless Communications*, vol. 12, no. 7, pp. 1–14, 2013.

- [6] X. Wu, S. Tavildar, S. Shakkottai, T. Richardson, J. Li, R. Laroia, and A. Jovicic, "FlashLinQ: A synchronous distributed scheduler for peer-to-peer ad hoc networks," *IEEE/ACM Transactions on Networking*, vol. 21, no. 4, pp. 1215–1228, 2013.
- [7] N. Naderializadeh and A. S. Avestimehr, "ITLinQ: A new approach for spectrum sharing in device-to-device communication systems," *IEEE Journal on Selected Areas in Communications*, vol. 32, no. 6, pp. 1139–1151, 2014.
- [8] X. Yi and G. Caire, "ITLinQ+: An improved spectrum sharing mechanism for device-to-device communications," in *2015 49th Asilomar Conference on Signals, Systems and Computers*. IEEE, 2015, pp. 1310–1314.
- [9] L. Song, Y. Li, and Z. Han, "Game-theoretic resource allocation for full-duplex communications," *IEEE Wireless Communications*, vol. 23, no. 3, pp. 50–56, 2016.
- [10] K. Shen and W. Yu, "FPLinQ: A cooperative spectrum sharing strategy for device-to-device communications," in *2017 IEEE International Symposium on Information Theory (ISIT)*. IEEE, 2017, pp. 2323–2327.
- [11] Z.-Q. Luo and S. Zhang, "Dynamic spectrum management: Complexity and duality," *IEEE Journal of Selected Topics in Signal Processing*, vol. 2, no. 1, pp. 57–73, 2008.
- [12] Y.-F. Liu and Y.-H. Dai, "On the complexity of joint subcarrier and power allocation for multi-user OFDMA systems," *IEEE Transactions on Signal Processing*, vol. 62, no. 3, pp. 583–596, 2013.
- [13] Y. Shen, J. Zhang, S. Song, and K. B. Letaief, "AI empowered resource management for future wireless networks," *arXiv preprint arXiv:2106.06178*, 2021.
- [14] H. Sun, X. Chen, Q. Shi, M. Hong, X. Fu, and N. D. Sidiropoulos, "Learning to optimize: Training deep neural networks for wireless resource management," in *2017 IEEE 18th International Workshop on Signal Processing Advances in Wireless Communications (SPAWC)*. IEEE, 2017, pp. 1–6.
- [15] M. Eisen, C. Zhang, L. F. Chamon, D. D. Lee, and A. Ribeiro, "Learning optimal resource allocations in wireless systems," *IEEE Transactions on Signal Processing*, vol. 67, no. 10, pp. 2775–2790, 2019.
- [16] Z. Wang, M. Eisen, and A. Ribeiro, "Unsupervised learning for asynchronous resource allocation in ad-hoc wireless networks," in *ICASSP 2021-2021 IEEE International Conference on Acoustics, Speech and Signal Processing (ICASSP)*. IEEE, 2021, pp. 8143–8147.
- [17] N. Naderializadeh, "Contrastive self-supervised learning for wireless power control," in *ICASSP 2021-2021 IEEE International Conference on Acoustics, Speech and Signal Processing (ICASSP)*. IEEE, 2021, pp. 4965–4969.
- [18] B. Song, H. Sun, W. Pu, S. Liu, and M. Hong, "To supervise or not to supervise: How to effectively learn wireless interference management models?" in *2021 IEEE 22nd International Workshop on Signal Processing Advances in Wireless Communications (SPAWC)*. IEEE, 2021, pp. 211–215.
- [19] N. Naderializadeh, "Wireless link scheduling via graph representation learning: A comparative study of different supervision levels," *arXiv preprint arXiv:2110.01722*, 2021.
- [20] A. Doshi, S. Yerramalli, L. Ferrari, T. Yoo, and J. G. Andrews, "A deep reinforcement learning framework for contention-based spectrum sharing," *IEEE Journal on Selected Areas in Communications*, 2021.
- [21] N. Naderializadeh, J. J. Sydir, M. Simsek, and H. Nikopour, "Resource management in wireless networks via multi-agent deep reinforcement learning," *IEEE Transactions on Wireless Communications*, vol. 20, no. 6, pp. 3507–3523, 2021.
- [22] I. Nikoloska and O. Simeone, "Fast power control adaptation via meta-learning for random edge graph neural networks," *arXiv preprint arXiv:2105.00459*, 2021.
- [23] S. He, S. Xiong, Y. Ou, J. Zhang, J. Wang, Y. Huang, and Y. Zhang, "An overview on the application of graph neural networks in wireless networks," *IEEE Open Journal of the Communications Society*, 2021.
- [24] Y. Shen, Y. Shi, J. Zhang, and K. B. Letaief, "A graph neural network approach for scalable wireless power control," *arXiv preprint arXiv:1907.08487*, 2019.
- [25] M. Eisen and A. Ribeiro, "Optimal wireless resource allocation with random edge graph neural networks," *IEEE Transactions on Signal Processing*, vol. 68, pp. 2977–2991, 2020.
- [26] M. Lee, G. Yu, and G. Y. Li, "Graph embedding-based wireless link scheduling with few training samples," *IEEE Transactions on Wireless Communications*, vol. 20, no. 4, pp. 2282–2294, 2020.
- [27] Z. Zhao, G. Verma, C. Rao, A. Swami, and S. Segarra, "Link scheduling using graph neural networks," *arXiv preprint arXiv:2109.05536*, 2021.
- [28] Z. Wang, M. Eisen, and A. Ribeiro, "Learning decentralized wireless resource allocations with graph neural networks," *arXiv e-prints*, pp. arXiv–2107, 2021.
- [29] I. Nikoloska and O. Simeone, "Black-box and modular meta-learning for power control via random edge graph neural networks," *arXiv preprint arXiv:2108.13178*, 2021.
- [30] L. F. Chamon, A. Amice, S. Paternain, and A. Ribeiro, "Resilient control: Compromising to adapt," in *59th IEEE Conference on Decision and Control (CDC)*. IEEE, 2020, pp. 5703–5710.
- [31] L. F. Chamon, S. Paternain, and A. Ribeiro, "Counterfactual programming for optimal control," in *Learning for Dynamics and Control*. PMLR, 2020, pp. 235–244.
- [32] A. Ribeiro, "Optimal resource allocation in wireless communication and networking," *EURASIP Journal on Wireless Communications and Networking*, vol. 2012, no. 1, pp. 1–19, 2012.
- [33] K. Hornik, M. Stinchcombe, and H. White, "Multilayer feedforward networks are universal approximators," *Neural Networks*, vol. 2, no. 5, pp. 359–366, 1989.
- [34] J. Bruna, W. Zaremba, A. Szlam, and Y. LeCun, "Spectral networks and locally connected networks on graphs," *arXiv preprint arXiv:1312.6203*, 2013.
- [35] M. Henaff, J. Bruna, and Y. LeCun, "Deep convolutional networks on graph-structured data," *arXiv preprint arXiv:1506.05163*, 2015.
- [36] M. Defferrard, X. Bresson, and P. Vandergheynst, "Convolutional neural networks on graphs with fast localized spectral filtering," *Advances in Neural Information Processing Systems*, vol. 29, 2016.
- [37] M. M. Bronstein, J. Bruna, Y. LeCun, A. Szlam, and P. Vandergheynst, "Geometric deep learning: going beyond euclidean data," *IEEE Signal Processing Magazine*, vol. 34, no. 4, pp. 18–42, 2017.
- [38] N. Keriven and G. Peyré, "Universal invariant and equivariant graph neural networks," *Advances in Neural Information Processing Systems*, vol. 32, 2019.
- [39] R. J. Williams, "Simple statistical gradient-following algorithms for connectionist reinforcement learning," *Machine learning*, vol. 8, no. 3, pp. 229–256, 1992.
- [40] R. S. Sutton, D. McAllester, S. Singh, and Y. Mansour, "Policy gradient methods for reinforcement learning with function approximation," *Advances in Neural Information Processing Systems*, vol. 12, 1999.
- [41] R. S. Sutton and A. G. Barto, *Reinforcement learning: An introduction*. MIT press, 2018.
- [42] X. Zhang and J. G. Andrews, "Downlink cellular network analysis with multi-slope path loss models," *IEEE Transactions on Communications*, vol. 63, no. 5, pp. 1881–1894, 2015.
- [43] J. G. Andrews, X. Zhang, G. D. Durgin, and A. K. Gupta, "Are we approaching the fundamental limits of wireless network densification?" *IEEE Communications Magazine*, vol. 54, no. 10, pp. 184–190, 2016.
- [44] Y. Li and X. Huang, "The simulation of independent Rayleigh faders," *IEEE Transactions on Communications*, vol. 50, no. 9, pp. 1503–1514, 2002.
- [45] H. S. Dhillon, R. K. Ganti, and J. G. Andrews, "Load-aware modeling and analysis of heterogeneous cellular networks," *IEEE Transactions on Wireless Communications*, vol. 12, no. 4, pp. 1666–1677, 2013.
- [46] E. Ranjan, S. Sanyal, and P. Talukdar, "ASAP: Adaptive structure aware pooling for learning hierarchical graph representations," *Proceedings of the AAAI Conference on Artificial Intelligence*, vol. 34, no. 04, pp. 5470–5477, 2020.
- [47] P. Viswanath, D. N. C. Tse, and R. Laroia, "Opportunistic beamforming using dumb antennas," *IEEE transactions on information theory*, vol. 48, no. 6, pp. 1277–1294, 2002.
- [48] M. Fey and J. E. Lenssen, "Fast graph representation learning with PyTorch Geometric," in *ICLR Workshop on Representation Learning on Graphs and Manifolds*, 2019.
- [49] N. Naderializadeh, O. Orhan, H. Nikopour, and S. Talwar, "Ultra-dense networks in 5G: Interference management via non-orthogonal multiple access and treating interference as noise," in *2017 IEEE 86th Vehicular Technology Conference (VTC-Fall)*. IEEE, 2017, pp. 1–6.
- [50] C. Geng, N. Naderializadeh, A. S. Avestimehr, and S. A. Jafar, "On the optimality of treating interference as noise," *IEEE Transactions on Information Theory*, vol. 61, no. 4, pp. 1753–1767, 2015.

APPENDIX A PROOF OF THEOREM 1

For notational convenience, we begin by restating the Lagrangian in (8) in a more compact form. To do so, we first

define the collected primal, unparameterized primal, and dual policies as $\tilde{\mathbf{p}}(\mathbf{H}) := [\mathbf{p}(\mathbf{H}); \gamma(\mathbf{H}); \mathbf{x}(\mathbf{H}); \mathbf{z}(\mathbf{H})]$, $\tilde{\mathbf{x}}(\mathbf{H}^\ell) := [\mathbf{x}(\mathbf{H}^\ell); \mathbf{z}(\mathbf{H}^\ell)]$, and $\tilde{\lambda}(\mathbf{H}^\ell) = [\lambda(\mathbf{H}^\ell); \mu(\mathbf{H}^\ell)]$. Further define $\boldsymbol{\theta}^p := [\boldsymbol{\theta}^p; \boldsymbol{\theta}^\gamma]$ to collect the RRM policy parameters. We can write the Lagrangian then as

$$\mathcal{L}_\theta(\boldsymbol{\theta}^p, \tilde{\mathbf{x}}, \tilde{\lambda}) = \mathbb{E}_{\mathbf{H}} \left[\mathcal{F}(\mathbf{H}, \tilde{\mathbf{x}}(\mathbf{H}^\ell)) - \tilde{\lambda}(\mathbf{H}^\ell)^T \mathcal{G}(\mathbf{H}; \boldsymbol{\theta}^p) \right]. \quad (42)$$

Observe we have further compacted the objective and constraint functions in $\mathcal{F}(\mathbf{H}, \tilde{\mathbf{x}}) := \mathcal{U}(\mathbf{x}(\mathbf{H}^\ell)) - \frac{\alpha}{2} \|\mathbf{z}(\mathbf{H}^\ell)\|_2^2$ and $\mathcal{G}(\mathbf{H}; \boldsymbol{\theta}^p) := [\mathbf{x}(\mathbf{H}^\ell) - \mathbf{f}(\mathbf{H}, \mathbf{p}(\mathbf{H}; \boldsymbol{\theta}^p), \gamma(\mathbf{H}; \boldsymbol{\theta}^\gamma)); f_{\min} - \mathbf{z}(\mathbf{H}^\ell) - \mathbf{x}(\mathbf{H}^\ell)]$, respectively.

The optimal parameterized dual value D_θ^* is given by the solution of the dual problem

$$D_\theta^* = \min_{\tilde{\lambda}} \max_{\boldsymbol{\theta}^p, \tilde{\mathbf{x}}} \mathbb{E}_{\mathbf{H}} \left[\mathcal{F}(\mathbf{H}, \tilde{\mathbf{x}}(\mathbf{H}^\ell)) - \tilde{\lambda}(\mathbf{H}^\ell)^T \mathcal{G}(\mathbf{H}; \boldsymbol{\theta}^p) \right]. \quad (43)$$

Given the fact that $\tilde{\mathbf{p}}(\mathbf{H}; \boldsymbol{\theta}^p)$ defines a subset of policies contained in the unparameterized class of policies in (5), the inner minimization in (43) can be upper bounded by

$$D_\theta^* \leq \min_{\tilde{\lambda}} \max_{\tilde{\mathbf{p}}} \mathbb{E}_{\mathbf{H}} \left[\mathcal{F}(\mathbf{H}, \tilde{\mathbf{x}}(\mathbf{H}^\ell)) - \tilde{\lambda}(\mathbf{H}^\ell)^T \mathcal{G}(\mathbf{H}, \tilde{\mathbf{p}}(\mathbf{H})) \right]. \quad (44)$$

The term on the right hand side of (44) indeed constitutes the unparameterized dual problem in (7). Due to strong duality of the original resilient RRM problem formulation—see [32, Theorem 1]—we know that $D^* = P^*$ and obtain the upper bound on D_θ^* in (14).

We proceed to derive the lower bound on D_θ^* . We add and subtract $\tilde{\lambda}(\mathbf{H}^\ell)^T \mathcal{G}(\mathbf{H}, \tilde{\mathbf{p}}^*(\mathbf{H}))$ to the right hand side of (43), where $\tilde{\mathbf{p}}^*(\mathbf{H})$ is the solution to the unparameterized primal problem in (5):

$$D_\theta^* = \min_{\tilde{\lambda}} \max_{\boldsymbol{\theta}^p} \mathbb{E}_{\mathbf{H}} \left[\mathcal{F}(\mathbf{H}, \tilde{\mathbf{p}}^*(\mathbf{H})) - \tilde{\lambda}(\mathbf{H}^\ell)^T \mathcal{G}(\mathbf{H}, \tilde{\mathbf{p}}^*(\mathbf{H})) \right] - \mathbb{E}_{\mathbf{H}} \left[\tilde{\lambda}(\mathbf{H}^\ell)^T (\mathcal{G}(\mathbf{H}; \boldsymbol{\theta}^p) - \mathcal{G}(\mathbf{H}, \tilde{\mathbf{p}}^*(\mathbf{H}))) \right]. \quad (45)$$

Observe in (45) that the first term on the right hand side does not involve the $\boldsymbol{\theta}^p$ and thus the maximization over $\boldsymbol{\theta}^p$ can be confined to the second term on the right hand side. Define the term $\Delta_\theta := \mathbb{E}_{\mathbf{H}} \left[\tilde{\lambda}(\mathbf{H}^\ell)^T (\mathcal{G}(\mathbf{H}; \boldsymbol{\theta}^p) - \mathcal{G}(\mathbf{H}, \tilde{\mathbf{p}}^*(\mathbf{H}))) \right]$ and lower bound the right hand side of (45) as

$$D_\theta^* \geq \min_{\tilde{\lambda}} \mathbb{E}_{\mathbf{H}} \left[\mathcal{F}(\mathbf{H}, \tilde{\mathbf{p}}^*(\mathbf{H})) - \tilde{\lambda}(\mathbf{H}^\ell)^T \mathcal{G}(\mathbf{H}, \tilde{\mathbf{p}}^*(\mathbf{H})) \right] - \min_{\boldsymbol{\theta}^p} |\Delta_\theta|. \quad (46)$$

We proceed to find an upper bound for $|\Delta_\theta|$. From Jensen's inequality we have that

$$|\Delta_\theta| \leq \mathbb{E}_{\mathbf{H}} \left| \tilde{\lambda}(\mathbf{H}^\ell)^T (\mathcal{G}(\mathbf{H}; \boldsymbol{\theta}^p) - \mathcal{G}(\mathbf{H}, \tilde{\mathbf{p}}^*(\mathbf{H}))) \right|. \quad (47)$$

We proceed to upper bound the term on the right hand side of (47) using Hölder's inequality, i.e.

$$|\Delta_\theta| \leq \mathbb{E}_{\mathbf{H}^\ell} \left\| \tilde{\lambda}(\mathbf{H}^\ell) \right\|_1 \mathbb{E}_{\mathbf{H}} \left\| \mathcal{G}(\mathbf{H}; \boldsymbol{\theta}^p) - \mathcal{G}(\mathbf{H}, \tilde{\mathbf{p}}^*(\mathbf{H})) \right\|_\infty. \quad (48)$$

A further upper bound can be made from (48) by applying

Lipschitz continuity of \mathcal{G} in Assumption 3 to obtain

$$|\Delta_\theta| \leq L_f \mathbb{E}_{\mathbf{H}^\ell} \left\| \tilde{\lambda}(\mathbf{H}^\ell) \right\|_1 \mathbb{E}_{\mathbf{H}} \left\| \tilde{\mathbf{p}}(\mathbf{H}; \boldsymbol{\theta}^p) - \tilde{\mathbf{p}}^*(\mathbf{H}) \right\|_\infty, \quad (49)$$

where $L_f := \max\{L_p, L_\gamma\}$. To upper bound the minimum of $|\Delta_\theta|$ over $\boldsymbol{\theta}^p$, consider that $\tilde{\mathbf{p}}(\cdot; \boldsymbol{\theta}^p)$ is a near-universal parameterization of degree $\epsilon_p := \max\{\epsilon_p, \epsilon_\gamma\}$. From (10), the parameterized primal policy can approximate $\tilde{\mathbf{p}}^*(\mathbf{H})$ to at least a degree of ϵ_p . From this we obtain

$$\min_{\boldsymbol{\theta}^p} |\Delta_\theta| \leq \epsilon_p \left(L_f \mathbb{E}_{\mathbf{H}^\ell} \left\| \tilde{\lambda}(\mathbf{H}^\ell) \right\|_1 \right). \quad (50)$$

Now, observe that the first term on the right hand side of (46) is given by the optimal unparameterized primal value P^* , while the second term on the right hand side is upper bounded using (50), giving us

$$D_\theta^* \geq P^* - \epsilon_p \left(L_f \mathbb{E}_{\mathbf{H}^\ell} \left\| \tilde{\lambda}(\mathbf{H}^\ell) \right\|_1 \right). \quad (51)$$

This completes the proof. \blacksquare

APPENDIX B PROOF OF PROPOSITION 1

Since the GNN operator Ψ consists of the composition of a sequence of L aggregation layers as in (24), it suffices to show that for any $l \in \{1, \dots, L\}$, the aggregation operation Ψ_l in (24) is permutation-equivariant. To that end, let $\mathbf{Y}^{l-1} = [\mathbf{y}_1^{l-1^T} \dots \mathbf{y}_n^{l-1^T}]^T \in \mathbb{R}^{n \times F_{l-1}}$ denote the array of node features at layer $l-1$ in the unpermuted graph. Also, let $\tilde{\mathbf{Y}}^{l-1} = [\tilde{\mathbf{y}}_1^{l-1^T} \dots \tilde{\mathbf{y}}_n^{l-1^T}]^T = [\mathbf{y}_{\pi(1)}^{l-1^T} \dots \mathbf{y}_{\pi(n)}^{l-1^T}]^T = \Pi \mathbf{Y}^{l-1}$ denote the array of node features at layer $l-1$ in the permuted graph, where $\pi : \mathcal{V} \rightarrow \mathcal{V}$ denotes the permutation operator corresponding to the permutation matrix Π . Moreover, for any node $v \in \mathcal{V}$, let $\tilde{\mathcal{N}}_v$ denote its 1-hop neighbors in the permuted graph, and for any edge (u, v) in the permuted graph, let $\tilde{w}(u, v)$ denote its weight. Then, ignoring the parameter vector $\boldsymbol{\theta}^l$ for brevity, for any node $v \in \mathcal{V}$ in the permuted graph, the feature vector at layer l can be written as

$$\begin{aligned} \tilde{\mathbf{y}}_v^l &= \Psi^l \left(\tilde{\mathbf{y}}_v^{l-1}, \tilde{w}(v, v), \{\tilde{\mathbf{y}}_u^{l-1}, \tilde{w}(u, v)\}_{u \in \tilde{\mathcal{N}}_v} \right) \\ &\stackrel{(a)}{=} \Psi^l \left(\mathbf{y}_{\pi(v)}^{l-1}, w(\pi(v), \pi(v)), \right. \\ &\quad \left. \left\{ \mathbf{y}_{\pi(u)}^{l-1}, w(\pi(u), \pi(v)) \right\}_{u \in \mathcal{V}: \pi(u) \in \mathcal{N}_{\pi(v)}} \right) \\ &\stackrel{(b)}{=} \Psi^l \left(\mathbf{y}_{\pi(v)}^{l-1}, w(\pi(v), \pi(v)), \left\{ \mathbf{y}_u^{l-1}, w(u, \pi(v)) \right\}_{u \in \mathcal{N}_{\pi(v)}} \right) \\ &\stackrel{(c)}{=} \mathbf{y}_{\pi(v)}^l, \end{aligned}$$

where (a) is true because for any node $v \in \mathcal{V}$ in the permuted graph, $\tilde{\mathcal{N}}_v = \{u \in \mathcal{V} : \pi(u) \in \mathcal{N}_{\pi(v)}\}$, and for any edge (u, v) in the permuted graph, $\tilde{w}(u, v) = w(\pi(u), \pi(v))$. Moreover, (b) holds due to a change of variables $u \leftarrow \pi(u)$, and (c) follows from the definition of the aggregation operator in (24) for node $\pi(v)$. This implies that $\tilde{\mathbf{Y}}^l = \Pi \mathbf{Y}^l$, i.e., the output feature vectors given the permuted inputs is the accordingly-permuted version of the output feature vectors in the unpermuted graph, hence completing the proof. \blacksquare